Integrated Optical Micromachined Pressure Sensors with Spectrally Encoded Output and Temperature Compensation

by

Gregory N. De Brabander, Glenn Beheim,* and Joseph T. Boyd

Department of Electrical and Computer Engineering and Computer Science
University of Cincinnati
Cincinnati, Ohio 45221-0030

Final Report

NASA Grant NAG 3-1774
Joseph T. Boyd, Principal Investigator

October, 1997

* NASA Lewis Research Center, MS 77-1, 21000 Brookpark Road, Cleveland, OH 44135

Integrated Optical Micromachined Pressure Sensor with Spectrally Encoded Output and Temperature Compensation

Gregory N. De Brabander[1], Glenn Beheim[2], and Joseph T. Boyd[3]

1. Department of Electrical and Computer Engineering and Computer Science, University of Cincinnati, Cincinnati, OH 45221-0030, now with Hewlett-Packard, San Jose, CA 95131
2. NASA Lewis Research Center, MS 77-1, 21000 Brookpark Road, Cleveland, OH 44135
3. Department of Electrical and Computer Engineering and Computer Science, University of Cincinnati, Cincinnati, OH 45221-0030

Abstract

A promising type of optical pressure sensor combines an integrated optical interferometer with a micromachined diaphragm on a shared silicon substrate. We have demonstrated a sensor of this type which uses an unbalanced Mach-Zehnder waveguide interferometer together with a broadband source to produce a spectrally encoded measurement. This spectral encoding mechanism is advantageous as it is not readily degraded by transmission through optical fibers. We have also demonstrated a means to obtain a temperature-compensated pressure measurement by interrogating both polarization eigenmodes of the interferometer.

Introduction

Fiber-linked optical sensors can provide substantial benefits in environments hostile to conventional electrical sensors, for example, in areas subject to high levels of electromagnetic radiation. Optical pressure sensors have been proposed which use a number of different stress-optical transduction mechanisms, such as modulation of the air gap of a Fabry-Perot interferometer by deflection of a diaphragm, [1,2] photoelastic modulation of polarization state,[3] interferometric detection of the stress-dependent resonant frequency of an optically excited vibrating beam,[4,5] and mechanical coupling of a diaphragm and integrated optical interferometer to produce photoelastic modulation of the interferometer optical path length difference (OPLD).[6-9]

A fiber optical pressure sensor based on the coupling of a micromachined diaphragm with integrated optical interrogation is most promising because of its robust monolithic construction, amenability to batch fabrication, and potential for high temperature operation. The pressure sensor of Ohkawa et al.[6] combined a micromachined silicon diaphragm with an integrated optical Mach-Zehnder interferometer so that monochromatic light coupled into the interferometer was intensity modulated as a function of pressure. A disadvantage of this type of sensor is the sensitivity of its intensity-coded output to changes in the transmissivity of the optical fiber link. In practice, large throughput changes can occur due to disturbances such as fiber bending, connector remating, and substitution of components.

In a previous paper we described a means to obtain a link-insensitive spectrally encoded pressure measurement using a sensor similar to the one fabricated by Ohkawa's group. An integrated optical ring resonator was fabricated on a micromachined silicon substrate such that a portion of the ring lay on top of the long edge of a narrow rectangular diaphragm and so was subject to a pressure-dependent strain. The pressure-indicating resonant frequency of the interferometer was determined using a frequency swept laser diode. A disadvantage of this sensor is its high sensitivity to temperature. Thermal sensitivity is proportional to the OPLD between interfering beams, which is necessarily large in the case of the ring. Although a Mach-Zehnder interferometer with arms of equal length[6,8,9] provides the lowest thermal sensitivity, a spectrally encoded output can be obtained only with an unbalanced interferometer. Here we report the use of an unbalanced Mach-Zehnder to provide a significantly reduced temperature sensitivity, in comparison to our previous spectrally encoded sensor. The reduced OPLD of this interferometer has necessitated the use of a different spectral interrogation method, which will be described. We will also outline a means to obtain temperature compensation by using the divergent pressure and temperature responses of the TE and TM modes of the interferometer.

Design and fabrication

Our sensor is shown schematically in Fig. 1. An integrated optical Mach-Zehnder interferometer, configured using single-mode channel waveguides, is fabricated in

dielectric layers on the top surface of a micromachined silicon wafer. A cavity has been etched from the back side of the wafer to produce a narrow rectangular diaphragm. The sensitivity to pressure is maximized by positioning one arm of the interferometer (the sensing arm) on top of one of the long edges of the diaphragm while the other arm (the reference arm) is remote from the diaphragm and unstressed. The physical length imbalance of the interferometer arms, $l_{reference} - l_{sense}$, is 100 μm. A difference in pressure across the diaphragm causes it to deflect, thereby imparting a stress to the waveguide on top of the diaphragm edge. Through the photoelastic effect, this stress alters the refractive index of the waveguide films, thereby altering the effective index of the guided mode, n_e, and the interferometer OPLD, Λ, as well, since

$$\Lambda = n_e\, l_{reference} - \int_{sensing\ arm} n_e(l)\, dl \quad . \tag{1}$$

The sensor is interrogated using the spectrally broadband emission from a superluminescent diode (SLD). The spectral power density of the light exiting the interferometer is given by

$$i_f(\lambda) = i_{SLD}(\lambda)\, T(\lambda)\, \frac{1}{2}\left[1 + \cos\left(\frac{2\pi\Lambda}{\lambda}\right)\right] \quad , \tag{2}$$

where $i_{SLD}(\lambda)$ is the SLD spectral power density and $[1-T(\lambda)]$ is the excess loss of the interferometer, which is essentially constant over the SLD spectral range. Pressure

induced changes in the OPLD are determined from the observed wavelength shifts of $i_t(\lambda)$. To facilitate this observation, the spectral range of the SLD emission should include at least one transmission maximum ($\lambda=\Lambda/m$, where m is an integer) and one minimum ($\lambda=\Lambda/(m+1/2)$). In other words, the free spectral range of the interferometer ($\sim\lambda^2/\Lambda$) should be less than the source spectral width. For a given source spectral width, this condition determines the minimum permissible interferometer imbalance.

Both the TM mode (light polarized perpendicular to substrate) and the orthogonally polarized TE mode of the interferometer are excited. As previously reported,[6,7] the OPLD of the TM mode, which is polarized parallel to the principal stress axis, is significantly more sensitive to pressure than is the OPLD of the TE mode. The thermal responses of both modes, however, are similar. The strongly divergent responses of the eigenmodes allows a determination of both temperature and pressure if the two OPLDs are measured simultaneously.

Fabrication

Figure 1 gives the physical dimensions of our sensor. We began with a 10 mil, <100>, double-side polished silicon substrate having a <110> flat. No etch stops were employed. The wafer was steam oxidized at 1050 °C for one day to grow a 3-μm thick oxide layer to mask the KOH etch. Using buffered HF and a photoresist mask, a rectangular hole, aligned with the flat, was etched in the back surface oxide. Subsequently,

the wafer was etched in 40°C KOH (Transene PSE-200) to form the diaphragm. The wafer was removed from the etch solution several times to monitor the etch progress. Early in the etch process, the depth of the etch pit was estimated using the movement required to focus a microscope alternately on the wafer back surface and the bottom of the etch pit. When the diaphragm was within ~20 μm of the desired thickness, its thickness was more precisely determined by measuring its transmission of a focused 0.633 μm HeNe laser beam. When the extinction coefficient of 0.01564 was used,[10] close agreement was obtained between the calculated thicknesses and those measured on cross sections by cleaving.

After the diaphragm was formed, the SiO_2 was stripped and regrown to a thickness of 2.98 μm. The silicon oxynitride film, with a refractive index of 1.513 at 0.63 μm, was deposited by low pressure chemical vapor deposition (LPCVD) using 20 sccm of $SiCl_2H_2$, 100 sccm of NH_3 and 11 sccm of O_2 at a pressure of 400 mTorr and a temperature of 750 °C.[11] Vacuum contact printing with infrared alignment to the edge of the diaphragm was used to pattern the photoresist and the ridges were wet etched using Timetch (Transene Co.). The upper cladding of SiO_2, with a refractive index of 1.451, was deposited using LPCVD at 300 mTorr with 10 sccm of $SiCl_2H_2$ and 40 sccm of N_2O at 910°C. According to both calculation and measurement, the channel waveguide supported only one TE and one TM mode at 830 nm.

Subsequent to waveguide fabrication, buffered HF was used to strip the films on the wafer back surface, except for the back of the diaphragm. The silicon chip was cleaved through the input and output channels to permit optical coupling. It was then aligned and electrostatically bonded to a 6-mm thick piece of Schott Borofloat glass. The glass had a diamond-drilled hole of 300 micrometers back-drilled to meet a 0.9 mm hole which penetrated all but 1.2 mm of the glass. The electrostatic bond was observed to be free of voids in the vicinity of the diaphragm. The sensor was bonded onto an aluminum chuck using epoxy, with a thin piece of compliant rubber between the glass and chuck to minimize thermal stresses.[12] To facilitate thermal testing a resistive heater and temperature sensor were mounted in the chuck.

Experimental Results

First, interferometer functionality was verified by coupling light from a SLD (GOLS 3000 from General Optronics Corp.) into the chip using microscope objectives. Since the SLD was weakly polarized, both the TE and TM modes were excited. The light exiting the interferometer was directed through a polarizer, for mode selection, to a scanning monochromator, which was used to analyze the output spectra of both modes. Fig. 2 shows $i_t(\lambda)$ of the TM mode. The TE output spectrum was similar. The output spectra for both modes were well described by Eq. 1, with Λ=150 μm.

To measure the sensor's temperature and pressure responses, the apparatus of Fig. 3 was used. This experimental setup allowed the rapid acquisition of the sensor's TE and TM output spectral power densities. Light from the SLD was collimated and passed through a polarizer before it was coupled into the chip. The input polarizer was used to equalize the TE and TM intensities. The light exiting the sensor was focused by another objective onto the entrance slit of a 0.25 m f/3.5 Ebert grating spectrometer. At the output of the spectrometer a polarizing cube beam splitter and mirror separated the two orthogonally polarized spectra. A CCD camera array, placed in the output focal plane of the spectrometer, was used together with a frame grabber to capture the two spectra which were subsequently transferred to a computer for analysis.

Figure 4 shows, for pressures ranging from 0 to 80 psi (552 kPa), the TE and TM output spectra after normalization by the SLD spectrum that was transmitted through a straight channel waveguide on the same chip. Pressure was increased from 0 to 80 psi in 20 psi increments, and then decreased back to 0. A discrete Fourier transform (DFT) algorithm was used over one cycle (73 pixels) to extract from each normalized spectra the phase of the fundamental sinusoid, and the phase changes were used to determine the OPLD changes relative to the initial measurement at 0 psi. Figure 5 shows, for both modes, the measured phase shifts $\Delta\Phi$ as functions of pressure, where $\Delta\Phi$ is related to the OPLD change $\Delta\Lambda$ by $\Delta\Phi = (2\pi/\lambda_{SLD})\,\Delta\Lambda$, where λ_{SLD} is the nominal SLD wavelength. The hysteresis of this sensor was found to be insignificant. The same techniques were

used to determine the phase change as a function of temperature. The measured phase sensitivities to pressure, P, and temperature, T, are given in Table 1.

Discussion

In agreement with theory,[6,7] the TM mode was found to be substantially more sensitive to pressure than was the TE mode, while the thermal responses of the two modes were found to be similar. The strong divergence of the TE and TM responses gives a well-conditioned system which permits the inversion of the matrix of table 1 to obtain ΔP and ΔT in terms of the TE and TM phase shifts:

$$\Delta P = (271 \text{ kPa/rad})\,\Delta\Phi_{TE} - (153 \text{ kPa/rad})\,\Delta\Phi_{TM} \qquad (3)$$

$$\Delta T = (88 \text{ °C/rad})\,\Delta\Phi_{TE} - (8.5 \text{ °C/rad})\,\Delta\Phi_{TM} \qquad (4)$$

Application of these equations to the calibration data yields RMS errors in ΔP and ΔT of 4 kPa and 0.8 °C. Analysis of this very limited data set is only intended to demonstrate the temperature-compensation process.

In summary, we have demonstrated an optical pressure that uses an unbalanced integrated optical Mach-Zehnder interferometer which is mechanically coupled to a micromachined silicon diaphragm and interrogated using a broadband solid state emitter.

The spectrally encoded output of this sensor provides a high degree of link immunity and its dual outputs allow for a temperature compensated pressure measurement.

Acknowledgments

The research described was supported in part by NASA grants NAG3-852 and NAG3-1774 and the NASA Space Engineering Research Center at the University of Cincinnati.

References

1. G. Beheim, K. Fritsch, and R. Poorman, "Fiber-linked Interferometric Pressure Sensor," Rev. Sci. Instrum. vol. 58, pp. 1655-1659 (1987).
2. R.A. Wolthuis, G.L. Mitchell, E. Saaski, J.C. Hartl, and M.A. Afromowitz, "Development of Medical Pressure and Temperature Sensors Employing Optical Spectrum Modulation," IEEE Transactions on Biomedical Engineering vol. 38, pp. 974-980 (1991).
3. G. Beheim and D.J. Anthan, "Fiber-Optic Photoelastic Pressure Sensor with Fiber-Loss Compensation," Opt. Lett. vol. 12, pp. 220-222 (1987).
4. D. Angelidis and P. Parsons, "Optical Micromachined Pressure Sensor for Aerospace Applications," Opt. Eng. vol. 31, pp. 1638-1641 (1992).
5. H. Unzeitig and H. Bartelt, "All-Optical Pressure Sensor with Temperature Compensation on Resonant PECVD Silicon Nitride Microstructures," Electronics Lett. vol. 28, pp. 400-402 (1992).
6. M. Ohkawa, M. Izutsu, and T. Sueta, "Integrated Optic Pressure Sensor on Silicon Substrate," Appl. Opt. vol. 28, pp. 5153-5157 (1989).
7. G.N. De Brabander, J.T. Boyd, and Glenn Beheim, "Integrated Optical Ring Resonator with Micromechanical Diaphragm for Pressure Sensing," IEEE Photonics Technology Letters vol. 6, pp. 671-673 (1994).
8. A. Vadekar, A. Nathan, and W. P. Huang, "Analysis and Design of an Integrated Silicon ARROW Mach-Zehnder Micromechanical Interferometer", J. Lightwave Technol. vol. 12, pp. 157-162 (1994).

9. K. Fischer, J. Müller, R. Hoffmann, F. Wasse, and D. Salle, "Elastooptical Properties of SiON Layers in an Integrated Optical Interferometer Used as a Pressure Sensor," J. Lightwave Technol. vol. 12, pp. 163-169 (1994).

10. J. Geist, A. R. Schaefer, J. F. Song, Y. H. Wang, and E. F. Zalewski, "An Accurate Value for the Absorption Coefficient of Silicon at 633 nm," J. of Res. Natl. Inst. Stand. Technol. vol. 95, pp. 549-558 (1990).

11. W. Gleine and J. Müller, "Low-Pressure Chemical Vapor Deposition Silicon-Oxynitride Films for Integrated Optics," Appl. Opt. vol. 31, pp. 2036-2040 (1992).

12. Y. Lin, P. Hesketh, J. Schuster, "Finite-element Analysis of Thermal Stresses in a Silicon Pressure Sensor for Various Die-Mount Materials," Sensors and Actuators vol. A 44, pp. 145-149 (1994).

Table 1. Phase and Temperature Sensitivities

Mode	$d\Phi/dP$ (rad/kPa)	$d\Phi/dT$ (rad/°C)
TE	- 0.00076	0.0137
TM	- 0.0079	0.0243

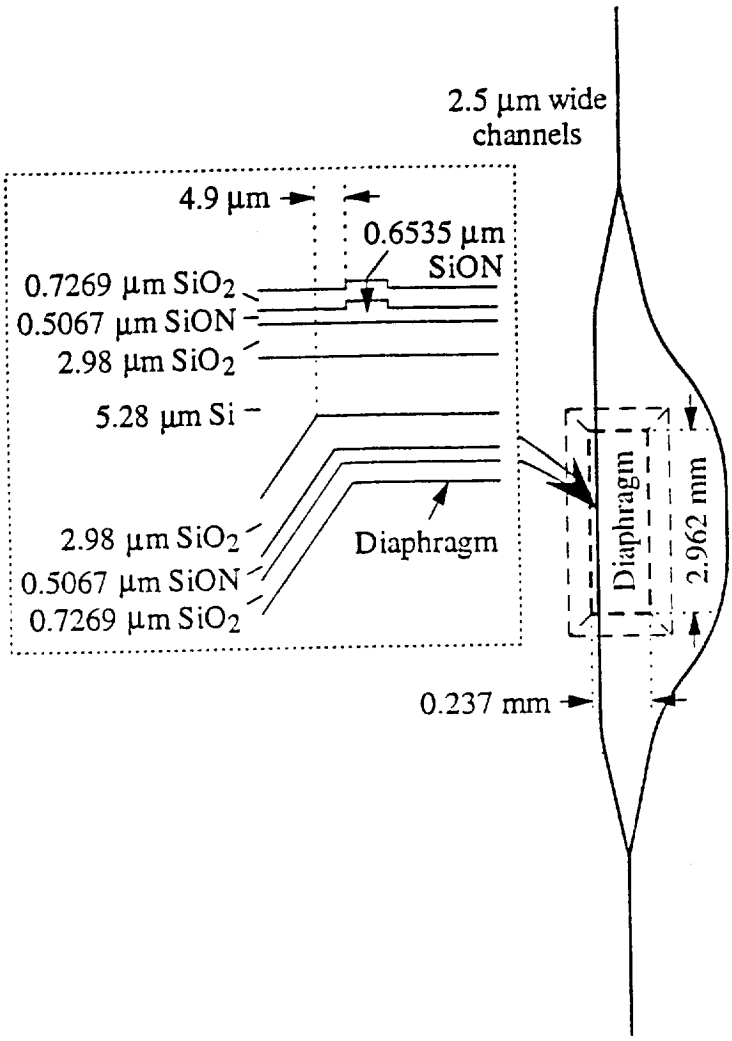
2.5 µm wide
channels
4.9 µm
0.6535 µm
SiON
0.7269 µm SiO2
0.5067 µm SiON
2.98 µm SiO2
5.28 µm Si
2.98 µm SiO2
0.5067 µm SiON
0.7269 µm SiO2
Diaphragm
Diaphragm
2.962 mm
0.237 mm

Figure 1

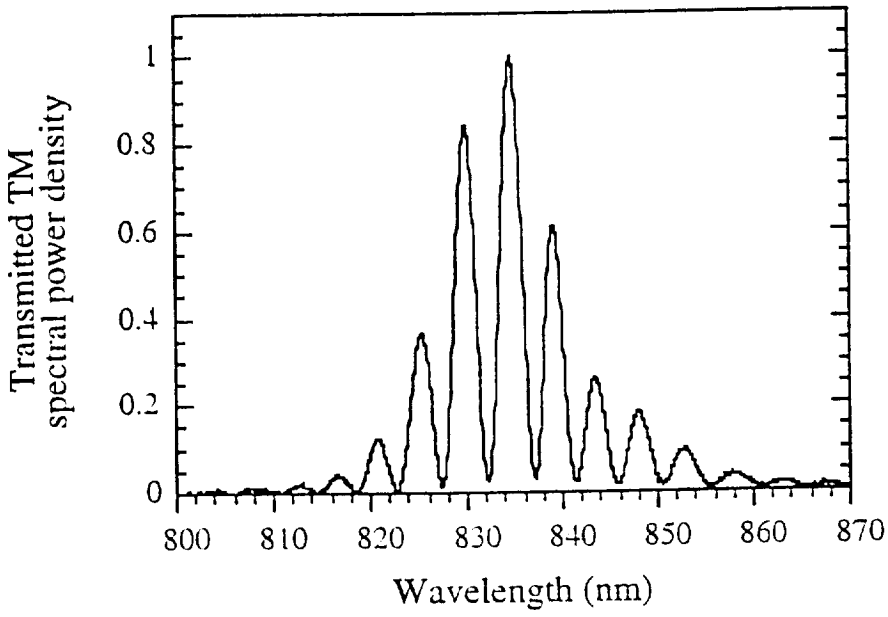
Transmitted TM
spectral power density
1
0.8
0.6
0.4
0.2
0
800
810
820
830
840
850
860
870
Wavelength (nm)

Figure 2

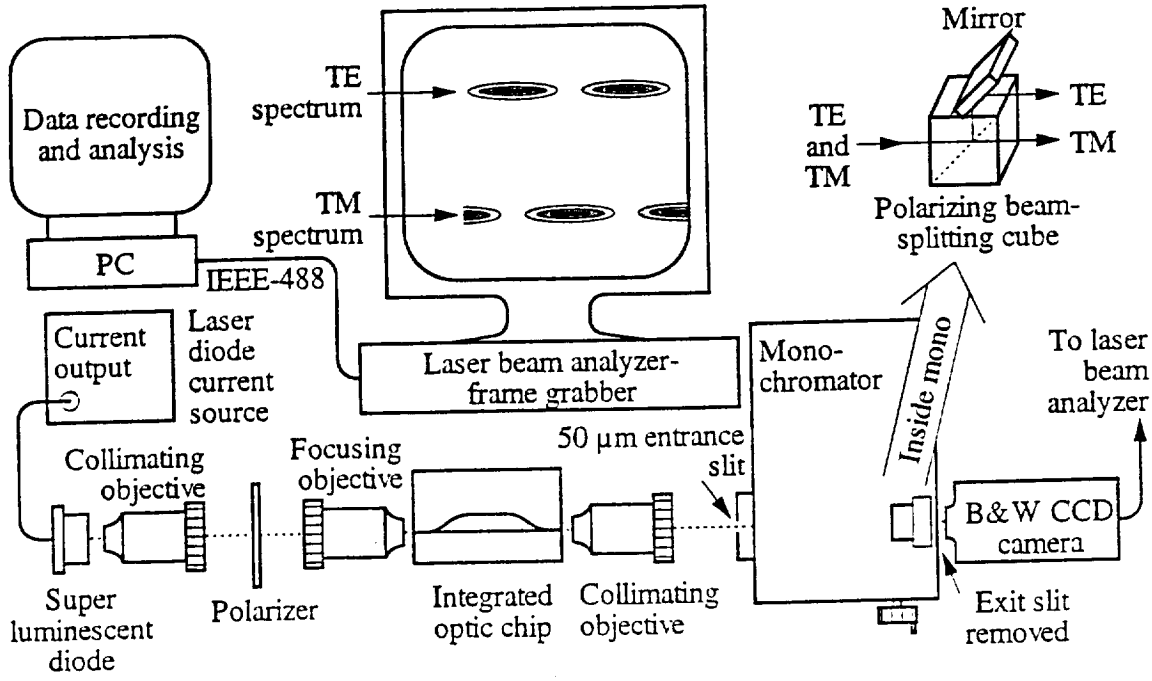
Data recording and analysis
PC
IEEE-488
TE spectrum
TM spectrum
Mirror
TE
TM
TE and TM
Polarizing beam-splitting cube
Current output
Laser diode current source
Laser beam analyzer-frame grabber
Mono-chromator
Inside mono
To laser beam analyzer
Collimating objective
Focusing objective
50 µm entrance slit
B&W CCD camera
Super luminescent diode
Polarizer
Integrated optic chip
Collimating objective
Exit slit removed

Figure 3

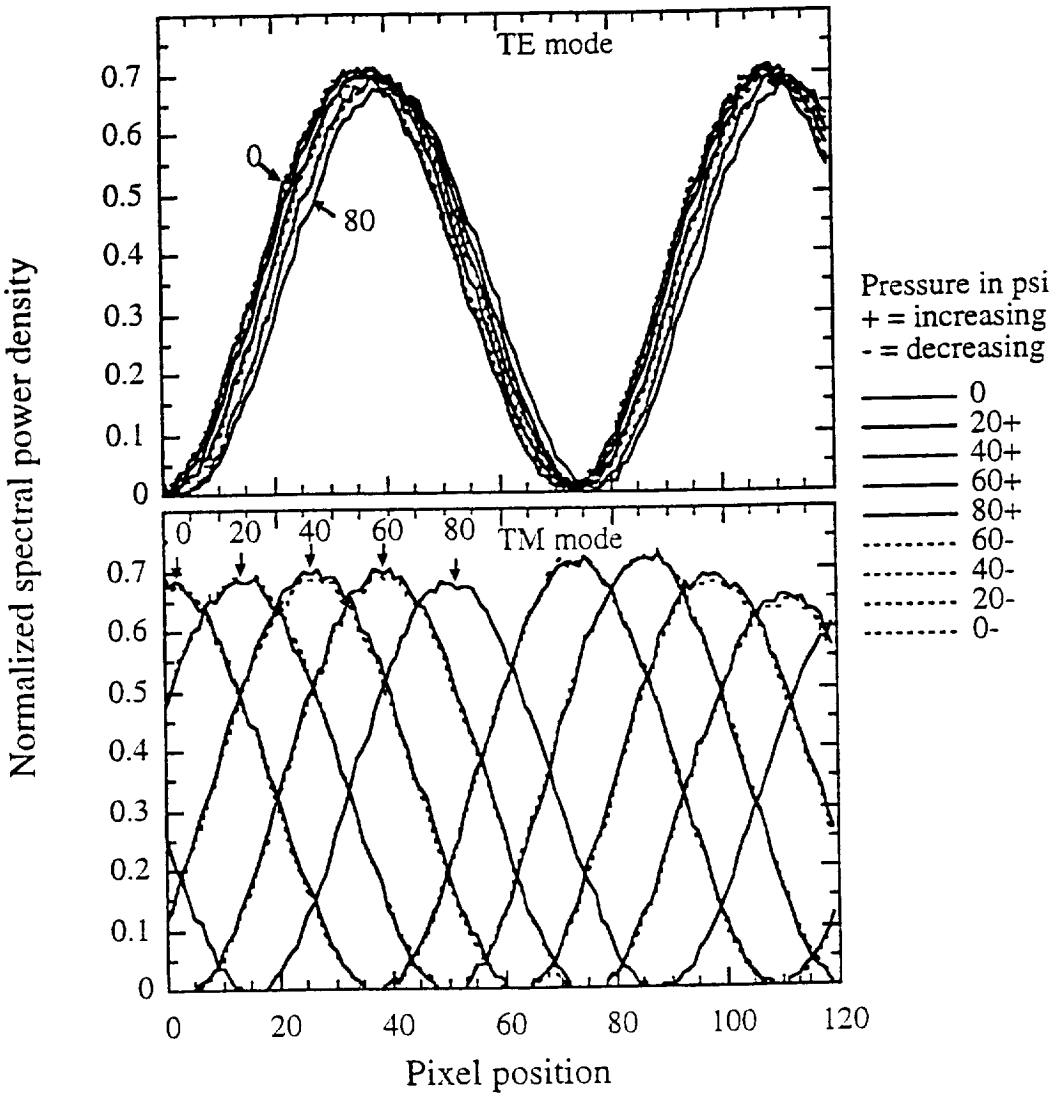
TE mode
TM mode
0
80
0 20 40 60 80
Normalized spectral power density
Pixel position
0.7
0.6
0.5
0.4
0.3
0.2
0.1
0
0 20 40 60 80 100 120
Pressure in psi
+ = increasing
- = decreasing
0
20+
40+
60+
80+
60-
40-
20-
0-

Figure 4

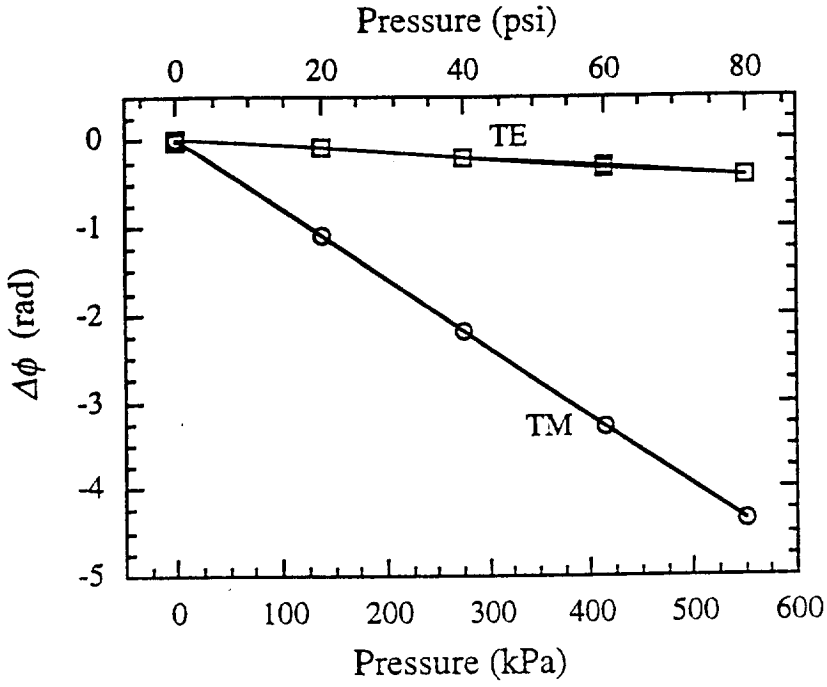
Pressure (psi)
0
20
40
60
80
0
-1
-2
-3
-4
-5
Δφ (rad)
TE
TM
0
100
200
300
400
500
600
Pressure (kPa)

Figure 5